Concentric Traveling Ionospheric Disturbances (CTID) Triggered by the 2022 Tonga Volcanic Eruption

Lei Liu[1], Y. Jade Morton[1], Pin-Hsuan Cheng[1], Angel Amores[2], Corwin J Wright[3], Lars Hoffmann[4]

1) Ann and H. J. Smead Aerospace Engineering Sciences Department, University of Colorado Boulder, Boulder, CO, US
2) Department of Physics, University of the Balearic Islands, Palma, Spain
3) Centre for Space, Atmospheric and Oceanic Science, University of Bath, Bath, UK
4) Jülich Supercomputing Center, Forschungszentrum Jülich, Jülich, Germany

Corresponding Author e-mail: lei.liu@colorado.edu

Key Points:

- Two distinctive types of concentric traveling ionospheric disturbances (CTID #1 and #2) were identified, and they propagated radially outward from Tonga at the speed of 610-880 m/s (acoustic-mode) and 300-380 m/s (Lamb-mode), respectively.
- The wavefront of the long-lasting CTID #2 changed after 08:35 UT over New Zealand, possibly due to the regional geomagnetic declination and westward-moving Lamb waves.
- Distinctive TEC enhancement of over 2 TECu magnitude observed above 530 km near the eruption site could be associated with the upward propagation of the acoustic-mode CTID #1 signatures in the F layer.

Abstract: This paper investigates concentric traveling ionospheric disturbances (CTID) associated with the Tonga volcanic eruption. Results show that: (1) Two types of CTID (CTID #1 and CTID #2) were identified that traveled radially from Tonga at the speed of 610-880 m/s (acoustic-mode) and 300-380 m/s (Lamb-mode), respectively. CTID #1 reached 3800 km and 5000 km away from the eruption location toward the directions of New Zealand and Australia, respectively. CTID #2 propagated persistently for ~9 hours over New Zealand and Australia. (2) The CTID #2 wavefront changed after 08:35 UT over New Zealand, possibly due to a combination of factors including the anisotropic propagation of CTID #2, the regional geomagnetic declination, and westward-moving Lamb waves. (3) Topside TEC enhancement with a magnitude over 2 TECu was observed from COSMIC-2 measurements. The enhancement agrees with CTID #1 peak from nearby ground-based TEC observations and could be related to the upward propagation of the F layer's CTID #1 signatures.

Plain Language Summary: The Tonga volcanic eruption on January 15 triggered various atmospheric waves that propagate from the Earth's surface and throughout the atmosphere and ionosphere. In this study, we discuss two types of concentric traveling ionospheric disturbances (CTID, #1 and #2) propagating outward from the Tonga site based on measurements collected by ~1000 ground-based global navigation satellite system (GNSS) receivers. Our analysis based on the CTID propagation speed showed that CTID #1 and #2 traveled at acoustic and Lamb wave modes, respectively. We also analyzed COSMIC-2 satellite radio occultation observations and showed that CTID #1-related enhancement signatures were observed at the topside ionosphere near the eruption site. Moreover, it is interesting to note that CTID #2 wavefront changed over New Zealand after 08:35 UT on January 15 likely followed the regional geomagnetic declination and westward-moving Lamb waves.

1 Introduction

Volcanic eruptions can generate a broad spectrum of atmospheric pressure waves, including acoustic, Lamb, and gravity waves. Acoustic waves propagate at the speed of ~330 m/s at the Earth's surface and increase to 800–1100 m/s in the ionosphere (Afraimovich et al., 2002; Heki,2006; Astafyeva, 2019; Aa et al., 2022). Lamb waves are a type of non-dispersive atmosphere waves that propagate horizontally above the Earth's surface with the speed of sound at ~300-350 m/s. However, they can cause ionospheric perturbations through energy leakage from the troposphere to the ionosphere (Ogawa et al., 1982; Mikumo et al., 1985; Kanamori et al., 1994; Heki, 2022; Zhang et al., 2022; Amores et al., 2022). Gravity waves propagate upward obliquely at a much lower velocity (50-250 m/s) than the sound speed and reach the ionosphere altitudes in ~45-60 minutes from the ground (Cheng and Huang, 1992; Artru et al., 2005; Dautermann et al., 2009; De et al., 2011; Miller et al., 2015; Wright et al., 2022).

On January 15, 2022, a volcanic eruption occurred at Hunga Tonga-Hunga Ha'apai (20.5°S, 175.1°W, hereafter simplified as Tonga) which triggered various atmospheric waves that propagate from the Earth's surface throughout the atmosphere (Amores et al., 2022; Wright et al., 2022; Carvajal et al., 2022; Otsuka,2022). Several researchers have presented interesting findings associated with this event. For example, Themens et al. (2022) identified two large-scale traveling ionospheric disturbances (TID)

and several subsequent mesoscale TIDs that propagated radially outward from the eruption site. Zhang et al. (2022) found the Lamb-mode TID traveled around the Earth three times. Lin et al. (2022) showed that concentric TIDs (CTID) were observed simultaneously over Australia and Japan because of the magnetic conjugate effect. Heki (2022) reported that ionospheric disturbances passed over Japan at least four times at the speed of Lamb waves, suggesting their origin as upward energy leakage from the troposphere. Aa et al. (2022a) observed prolonged equatorial plasma bubbles over the Asia-Oceania area following the arrival of Lamb waves. Astafyeva et al. (2022) estimated the Tonga eruption onset time and the released energy based on ionospheric TEC observations. Saito (2022) observed two types of TIDs that arrived over Japan about 3 and 7 hours after the eruption, respectively. Aa et al. (2022b) observed dramatic suppression and deformation of the equatorial ionization anomaly (EIA) crests occurred in the American sector after the Tonga volcano eruption. Ghent and Crowell (2022) detected supersonic acoustic, Lamb, and tsunami signals over the southwestern Pacific using GNSS ionospheric observables.

In this study, we present additional observations of new features and analysis of the volcanic-induced ionospheric effects. Using ground-based GNSS network measurements, we observed the presence of two distinctive types of CTIDs. This is the first time the CTID wavefront change is observed over New Zealand. Moreover, topside ionospheric TEC enhancement near the eruption site is reported for the first time from low Earth orbit (LEO)-based COSMIC-2 observations.

2 Data and Methodology

Global navigation satellite system (GNSS) total electron content (TEC) observations used in this study are calculated from ~1000 GNSS (GPS/GLONASS/BDS) receivers at a 30-second sampling rate. These receivers are operated by the International GNSS Service (IGS) (Beutler et al., 1999), University NAVSTAR Consortium (UNAVCO) (Ware et al., 2000), New Zealand GeoNet, and Australia GNSS networks and are located in the region (50°S-10°N, 110°E-160°W). Figure S1 in the supporting information (SI) file shows the locations of these receivers. An elevation mask of 15° from GNSS receivers to satellites is used to mitigate potential multipath effects. The ionospheric piercing point (IPP) height is set to be 300 km, which is around the height of the F2-layer peak electron density (hmF2) according to radio occultation electron density profiles. Taking advantage of the quasi-invariant orbital location of the BDS geostationary earth orbit (GEO) satellites C01, C03 and C04, ionospheric TEC observations from BDS GEO receiver-satellite pairs are also used in this study to provide ionospheric observations without being influenced by ionospheric spatiotemporal variations. To extract traveling ionospheric disturbances (TID) signals from GNSS TEC observations, the detrended TEC (dTEC) is obtained by applying a Savitzky-Golay filter with a 40-minute sliding window (Savitzky and Golay, 1964; Zhang et al., 2017). The constellation observing system for meteorology, ionosphere, and climate (COSMIC)-2 precise orbit determination (pod) TEC (podTEC) measurements, which are TEC values above the LEO orbit altitude (550 km), were used to measure the response of the topside ionosphere. It should be noted that only podTEC for elevation angles of the LEO-GPS link larger than 0° are used in this study. In addition, infrared radiance (IR) imagery data from the 10.3 channel of the geostationary operational environmental satellite (GOES)-17 were used to investigate the volcano-related Lamb wave

propagation in the lower atmosphere (30 km). GOES-17 is a geostationary satellite located above (0°,137.2°W) at an orbit altitude of ~36000 km. It provides images of the Pacific region at spatial and temporal resolutions of 2 km and 10 minutes, respectively (Schmit et al., 2017). To visualize the Lamb wave structures from GOES-17 IR data, filter processing is applied in both temporal and spatial domains to obtain the filtered IR observations (Amores et al., 2018 and 2022).

3 Results

3.1 Observations Using Ground-based GNSS Networks Near New Zealand and Australia

Figure 1 shows two-dimensional (2D) detrended TEC (dTEC) maps at nine selected time steps on January 15, 2022. Full sets of 2D dTEC maps with a 15-minute interval are available in Movie S1 in the SI file. Two distinctive CTIDs are characterized by different propagation speeds and will be analyzed in detail in Figure 2. We denote the two CTIDs as CTID #1 and CTID #2, which are marked by black arrows in Figure 1.

CTID #1 propagated radially outward from the Tonga eruption location and arrived over New Zealand (2000-2500 km from the epicenter at 05:25 UT. The wavefronts of CTID #1 are aligned with the magenta dashed line of great circles centered on the eruption. From 05:25 to 06:05 UT (see Movie S1 and Figures 1(a)-1(c)), CTID #1 propagated past New Zealand and its aptitude became attenuated at around 3500-4000 km from the epicenter. Signatures matching that of CTID #1 reached the Australia sector (~140°E-150°E) at 06:40 UT (Figure 1(e)). CTID #1 continued propagating outward at 06:55 UT (Figure 1(f)) and disappeared around 5000 km away from the epicenter over Australia. After 06:20 UT, CTID #2 started to appear in New Zealand and propagated radially outward over 4000 km away (see Figures 1(d)-1(i) and Movie S1). After 07:45 UT (see Figures 1(g)-1(i) and Movie S1), clear CTID #2 signatures were simultaneously observed over New Zealand and Australia and propagated outward persistently for around 9 hours. It is interesting to note that the wavefront of CTID #2 in New Zealand is generally aligned with the magenta dashed lines before 08:35 UT, but it comes into alignment with the black dashed lines after 08:35 UT. The center of the black dashed curves (shown as a black cross) is located at (21.1°S, 178.6°E), which is west of the epicenter (20.5°S, 175.1°W). The IPP of the black cross is 660 km away from the IPP of the magenta star. The change in CTID #2 wavefront will be further discussed in section 4.

Figure 2(a) shows the sound speed profile over a range of altitudes calculated from the Naval Research Laboratory Mass Spectrometer and Incoherent Scatter Radar Exosphere (NRLMSISE-00) model (Picone et al., 2002). According to the model, the theoretical propagation speed at 30 km (the lamb-mode in the lower atmosphere) and 300 km (acoustic-mode in the ionosphere) is 321.7 m/s and 822.4 m/s, respectively. Figures 2(c) and 2(d) show the dTEC plotted in UT vs. distance over New Zealand and Australia, respectively. The distances are calculated from related IPP locations to the

epicenter at 300 km altitude. IPP tracks used for generating Figures 2(c) and 2(d) are marked by blue curves and red crosses in Figure 2(b), respectively.

We estimated the CTID propagation speed by tracing the slope of positive and negative wave structures using linear regression in the UT-distance plots. Two groups of CTIDs (#1 and #2) were observed over both the New Zealand and Australia regions (see oblique dashed yellow and green lines in Figures 2(c) and 2(d)). In Figure 2(c), CTID #1 appeared around 05:25-06:30 UT at a speed of 700-860 m/s over New Zealand and propagated as far as 3500-3800 km away from the epicenter around 06:30-06:50 UT at a decreased speed of ~610 m/s. CTID #2 started to appear at 06:20 UT around 2300 km from the epicenter and continued propagating outward over and beyond New Zealand at a speed of 300-380 m/s and lasting for ~9 hours. In Figure 2(d), clear CTID #1 waves propagated 3800-5000 km, reaching Australia at a speed of 700-880 m/s during 06:20-07:40 UT. CTID #1 over Australia was mixed with CTID #2 within 5000 km after 07:40 UT and became weakened and disappeared gradually by 08:00 UT. After 08:00 UT, CTID #2 dominated with persistency at a speed of 340-360 m/s for more than 9 hours over Australia.

According to our speed estimation from the waves over New Zealand and Australia, CTID #1 propagated at approximately 610-880 m/s, which matches the theoretical acoustic speed (822.4 m/s) in the ionosphere from the NRLMSISE-00 model. It reached as far as 5000 km reaching Australia from the volcanic eruption location. CTID #2 traveled with a speed of 300-380 m/s in the ionosphere and lasted for around 9 hours over New Zealand and Australia. The propagation speed of CTID #2 is close to the Lamb wave speed (321.7 m/s) in the lower atmosphere derived from the NRLMSISE-00 model. We note that the dTEC magnitudes shown in Figures 1 and 2 are presented with saturated color scales to provide a clear visualization of TID wavefronts. The real dTEC amplitudes are generally larger than those shown in Figures 1 and 2 (see Figure S3 in the SI file for details).

3.2 Observations using BDS GEO Satellite Measurements

In addition to the CTID #1 signatures over New Zealand and Australia, slant TEC (sTEC) observations from BDS GEO C01 and C04 satellites are used to verify CTID #1 signatures detected within 3000 km, except for New Zealand. Figure 3(a) shows BDS GEO IPP locations at the azimuth of -135° to 90° within 3000 km from the eruption. Related GNSS receivers are marked by black dots. Figure 3(b) shows a randomly selected sTEC time series during 04:00-10:00 UT from the line of sight between GNSS receiver TUVA and BDS GEO satellite C01. This sTEC is in general decreasing. However, there are two clearly identifiable local minima as marked by black and blue circles, respectively. The third point of interest (red circle) is the beginning of the steep drop in sTEC, which led to the first local minimum. We identified similar local minima and the beginning of the steep drop of sTEC for all sTEC profiles computed from the BDS GEO C01 and C04 measurements. Figure 3(c) plots the IPP distances from the epicenter against universal time (UT) for these three types of data points of interest. Propagation speeds are estimated by fitting the slope using linear regression from these three types of data points. Results show that the speeds estimated from dashed red, black, and blue lines (see Figure 3(c)) are all within 690-760 m/s, agreeing well with the CTID #1 speed derived from Figure 2. This

means that the ionosphere perturbations here (Figure 3) and for CTID #1 over New Zealand and Australia (Figure 2) are the manifestation of the same TID in different azimuth directions. This also confirms the radial propagation of CTID #1 from Tonga.

3.3 COSMIC-2 Ionospheric Observations

Figure 4(a) shows the paths of the LEO-based COSMIC-2 E2 satellite in the vicinity of the eruption site over the Pacific Ocean on January 14 (cyan curve) and January 15 (blue curve). Topside TEC values above the LEO satellite orbit (~530 km) derived from GPS G32 during 05:00-05:30 UT are plotted in Figure 4(b). A topside TEC enhancement exceeding 2 TECu was detected in Figure 4(b) around 05:01-05:15 UT on January 15. Similar topside ionospheric TEC enhancement structures were also observed for other COSMIC-GPS links (see Figures S4-S6 of the SI file). No discernible topside ionospheric enhancement can be identified on January 14. In Figure 4(d), the TEC from ground-based BDS GEO C01 and C04 satellites increased sharply around 05:10-05:40 UT at nearby locations where the LEO-based topside TEC enhancement structures were observed. Moreover, clear TEC enhancements can be also observed from available GNSS stations distributed nearly 1000-1500 km from the volcanic eruption location during 05:00-06:00 UT on January 15, 2022 (see Figures S7 and S8 of the SI file). This indicates that TEC enhancements observed at the topside ionosphere and F layer height are correlated. It should be noted that the enhancements observed from the ground-based TEC data are at roughly the same time align the same great circle where the CTID #1 signals were detected, so the LEO-based topside TEC enhancement is probably associated with CTID #1 of the F layer.

3.4 Comparison with GOES-17 Observations

Figure 5 compares the arrival time of the CTID #2 and the Lamb waves when they first reached New Zealand and Australia. The arrival of CTID #2 observed from dTEC maps over New Zealand at 06:25 UT is shown in Figure 5(a), and the arrival time of the earliest Lamb wave captured by the GOES-17 filtered IR image in the same region is shown in Figure 5(b). There is a close agreement between CTID #2 and Lamb waves in New Zealand in terms of arrival time, occurrence location, and spatial pattern (see red arrows in panels (a) and (b)). Similarly, the CTID #2 observed over Australia at 07:45 UT is well-aligned with the presence of the Lamb wave (see black arrows in panels (c) and (d)). These indicate that CTID #2 is indeed associated with the propagation of the volcano-induced Lamb waves in the lower atmosphere.

4 Discussion and Conclusion

Based on ground-based GNSS and LEO-based COSMIC-2 measurements, we identified two types of CTID, CTID #1 and CTID #2, associated with the Tonga volcanic eruption on January 15, 2022. The change of CTID wavefronts over New Zealand and the topside ionospheric TEC enhancement near the eruption location are summarized below.

(1) According to the speed estimation over New Zealand (Figure 2(c)), Australia (Figure 2(d)), and the Pacific Ocean (Figure 3), CTID #1 propagated radially at 610-880 m/s, which is close to the theoretical acoustic velocity (822.4 m/s) at the ionospheric height calculated from the NRLMSISE-00 model. Afraimovich et al. (2002), Heki (2006), and Astafyeva (2019) reported that the velocity of shock acoustic waves in the ionosphere is 600-1100 m/s, which is consistent with the CID #1 speed estimated in this study. These suggest that the shock acoustic waves induced by the volcanic explosion reached ionospheric altitudes and produced CTID #1, though further study is still needed to characterize the CTID #1 period which is expected to be less than the buoyancy period (Astafyeva, 2019). Moreover, CTID #1 propagated outward from the volcanic eruption location as far as 3800 km and 5000 km away to reach New Zealand and Australia, respectively. To our best knowledge, it is the first time that the acoustic-mode CTID associated with the volcanic eruption has been observed to propagate such a long distance.

(2) The prevailing CTID #2 propagated persistently for around 9 hours over New Zealand and Australia at a speed of 300-380 m/s (Figure 2), which is consistent with the speed estimated by Lin et al. (2022), Zhang et al. (2022) and Themens et al. (2022) for this event. According to Amores et al. (2022) and Otsuka (2022), the Lamb wave triggered by the Tonga volcanic explosion travelled globally. Its propagation speed in the lower atmosphere, estimated by the NRLMSISE-00 model, is 321.7 m/s (Figure 2(a)), and from surface pressure and stratospheric nadir sounder observations is 310-320 m/s (Wright et al., 2022). The similarities in propagation speed suggest that the CTID #2 in the ionosphere is driven by the volcano-induced Lamb wave from the lower atmosphere. Moreover, the Lamb wave captured by the GOES-17 IR data shows a similar spatial pattern and arrival time with the CTID #2 over New Zealand and Australia. This also shows evidence that the presence of CTID #2 is related to Lamb waves. CTID #2 could be caused by the upward energy leakage into the ionosphere from Lamb waves either via resonance with the atmosphere during propagation (Zhang et al., 2022; Heki, 2022; Ogawa et al., 1982) or by the stimulation of gravity waves that are excited by the Lamb waves and ultimately travel at a propagation speed similar to Lamb waves in the troposphere (Lin et al., 2022).

(3) The wavefronts of Lamb-mode CTID #2 over New Zealand before 08:35 UT are mostly aligned with a great circle (magenta dashed line in Figure 1). After 08:35 UT, the wavefront is aligned with a different great circle (black dashed line in Figure 1), which is located about 660 km west of the epicenter. The change of the CTID #2 wavefront could be related to various factors:

- As the TID propagated outward for long distances, their wavefront may have shifted from the

original shape because of the anisotropic propagation characteristics of waves. Moreover, the polarization electric field (PEF) is generated in association with the TIDs (Huang et al., 1994; Tsunoda, 2010; Zhang et al., 2019 and 2021). We believe that the PEF embedded in the CTID #2 before 08:35 UT was able to help maintain the propagation direction of the original CTIDs. However, the CTID #2 after 08:35 UT over New Zealand was characterized by smaller fluctuation amplitudes than before (see Figure 3(b) in Zhang et al. (2022)), suggesting that the PEF was weakened to a level that it could no longer maintain the TID original propagation direction. Subsequent TID propagation over New Zealand would be guided by the distribution of the regional geomagnetic field lines where the geomagnetic declination is around 22-26°. The geomagnetic declination is visually close to the CTID #2 propagation direction after the wavefront change. Therefore, the regional geomagnetic declination could be an important factor responsible for the CTID #2 wavefront change when the PEF embedded in the CTID #2 gradually dissipated. Further study is still needed to investigate the quantitative relationship between the CTID #2 wavefront change and geomagnetic declination.

- In addition to regional geomagnetic declination, the westward-moving Lamb waves could further contribute to the wavefront change. The ionospheric disturbance center of CTID #2 coincides well with the source center of the concentric Lamb waves from the GOES-17 filtered IR (see Figures 5(b) and 5(d)) and AIRS brightness temperature perturbation measurements (see Figure S9 of the SI file). Wright et al. (2022) also observed that the Lamb wave center was slightly to the west of the eruption and moved further westward driven by prevailing easterly winds in the lower atmosphere. These suggest that the westward-moving Lamb waves could also be responsible for the CTID #2 wavefront change though its impacts could be secondary. Our investigation shows that the dusk terminator (see Movies S2 and S3 in the SI file) and ionospheric shell heights (see Figure S10 in the SI file) have negligible effects on the CTID #2 wavefront change observed in this study. However, we caution the reader that the wave activity at dusk has its day-to-day variability. Therefore, the analysis on other days can only provide background references but not rigorous evidence of the negligible effects of the dusk terminator on the wavefront change.

(4) The TEC enhancement structures were simultaneously observed by ground-based BDS GEO TEC (Figures 3(b) and 4(d), and Figures S7-S8 of the SI file) and LEO-based COSMIC-2 podTEC (Figure 4(b) and Figures S4-S6) measurements. This means that this enhancement is the same structure that appeared at both the F-layer ionosphere (300 km) and the topside ionosphere (above 530 km). From Figure 3, we know that the clear TEC enhancement before 06:00 UT is a manifestation of the CTID #1 peak in the F layer, so the LEO-based TEC enhancement is likely to be the signature of the CTID #1 in the topside ionosphere (above 530 km) through the upward propagation of CTID #1.

Acknowledgments

This project is sponsored by NASA grant 80NSSC21K1156. CJ Wright is supported by a Royal Society University Research Fellowship (UF160545 and URF\R\221023) and NERC grant NE/S00985X/1. The authors are grateful for the constructive comments provided by the anonymous reviewers and for the useful discussion with Dr. Ercha Aa and Dr. Weijia Zhan in revising the manuscript.

The GNSS data used in this study are available from University NAVSTAR Consortium (UNAVCO) (https://data.unavco.org/archive/gnss/), Crustal Dynamics Data Information System (CDDIS) (https://cddis.nasa.gov/), New Zealand GeoNet (https://data.geonet.org.nz/gnss/), Australia GNSS networks (https://gnss.ga.gov.au/network), respectively. The constellation observing system for meteorology, ionosphere, and climate (COSMIC)-2 podTEC measurements are available from https://data.cosmic.ucar.edu/gnss-ro/cosmic2/. The Geostationary Operational Environmental Satellite (GOES)-17 infrared radiance data are from https://home.chpc.utah.edu/~u0553130/Brian_Blaylock/cgi-bin/goes16_download.cgi. The Advanced Infrared Sounder (AIRS) aboard NASA's Aqua satellite brightness temperature perturbation data are from https://datapub.fz-juelich.de/slcs/airs/gravity_waves/data/projects/tonga/.

Reference

[1] Aa, E., Zhang, S.-R., Erickson, P. J., Vierinen, J., Coster, A. J., Goncharenko, L. P., et al. (2022a). Significant ionospheric hole and equatorial plasma bubbles after the 2022 Tonga volcano eruption. Space Weather, 20, e2022SW003101. https://doi.org/10.1029/2022SW003101

[2] Aa, E., Zhang, S.-R., Wang, W., Erickson, P. J., Qian, L., Eastes, R., et al. (2022b). Pronounced suppression and X-pattern merging of equatorial ionization anomalies after the 2022 Tonga volcano eruption. Journal of Geophysical Research: Space Physics, 127, e2022JA030527. https://doi.org/10.1029/2022JA030527

[3] Afraimovich, E. L. (2008), First GPS-TEC evidence for the wave structure excited by the solar terminator, Earth Planets Space,60, 895–900.

[4] Afraimovich, E. L., Kosogorov, E. A., & Plotnikov, A. V. (2002). Shock–acoustic waves generated during rocket launches and earthquakes. Cosmic Research, 40(3), 241–254. https://doi.org/10.1023/A:1015925020387

[5] Amores, A., Jordà, G., Arsouze, T., & Le Sommer, J. (2018). Up to what extent can we characterize ocean eddies using present-day gridded altimetric products? Journal of Geophysical Research: Oceans, 123(10), 7220-7236.

[6] Amores, A., Monserrat, S., Marcos, M., Argüeso, D., Villalonga, J., Jordà, G., & Gomis, D. (2022). Numerical simulation of atmospheric Lamb waves generated by the 2022 Hunga‐Tonga volcanic eruption. Geophysical Research Letters, e2022GL098240.

[7] Artru, J., Ducic, V., Kanamori, H., Lognonné, P., & Murakami, M. (2005). Ionospheric detection

of gravity waves induced by tsunamis. Geophysical Journal International, 160(3), 840-848.

[8] Astafyeva, E. (2019). Ionospheric detection of natural hazards. Reviews of Geophysics, 57(4), 1265-1288.

[9] Astafyeva, E., Maletckii, B., et al. (2022) The 15 January 2022 Hunga Tonga eruption history as inferred from ionospheric observations, ESSOAr, doi: 10.1002/essoar.10511226.1, https://doi.org/10.1002/essoar.10511226.1

[10] Beer, T. (1978). On atmospheric wave generation by the terminator. Planetary and Space Science, 26(2), 185-188.

[11] Carvajal, M., Sepúlveda, I., Gubler, A., & Garreaud, R. (2022). Worldwide signature of the 2022 Tonga volcanic tsunami. Geophysical Research Letters, e2022GL098153.

[12] Cheng K, Huang YN (1992) Ionospheric disturbances observed during the period of Mount Pinatubo eruptions in June 1991. J Geophys Res 97(A11):16995. doi:10.1029/92JA01462

[13] Dautermann, T., Calais, E., Lognonné, P., & Mattioli, G. S. (2009). Lithosphere-atmosphere-ionosphere coupling after the 2003 explosive eruption of the Soufriere Hills Volcano, Monserrat. Geophysical Journal International, 179(3), 1537–1546. https://doi.org/10.1111/j.1365-246X.2009.04390.x

[14] De Angelis, S., McNutt, S. R., & Webley, P. W. (2011). Evidence of atmospheric gravity waves during the 2008 eruption of Okmok volcano from seismic and remote sensing observations. Geophysical Research Letters, 38(10).

[15] Forbes, J. M., S. L. Bruinsma, Y. Miyoshi, and H. Fujiwara (2008), A solar terminator wave in thermosphere neutral densities measured by the CHAMP satellite, Geophys. Res. Lett.,35, L14802, doi:10.1029/2008GL034075

[16] Ghent, J. N., & Crowell, B. W. (2022). Spectral characteristics of ionospheric disturbances over the southwestern Pacific from the 15 January 2022 Tonga eruption and tsunami. Geophysical Research Letters, 49, e2022GL100145. https://doi.org/10.1029/2022GL100145

[17] Heki, K. (2006). Explosion energy of the 2004 eruption of the Asama Volcano, central Japan, inferred from ionospheric disturbances. Geophysical Research Letters, 33(14).

[18] Heki, K. (2022). Ionospheric signatures of repeated passages of atmospheric waves by the 2022 Jan. 15 Hunga Tonga eruption detected by QZSS-TEC observations in Japan. DOI: https://doi.org/10.21203/rs.3.rs-1448599/v1

[19] Huang, C.-S., C. A. Miller, and M. C. Kelley (1994), Basic properties and gravity wave initiation of the midlatitude F region instability, Radio Sci., 29, 395–405, doi:10.1029/93RS01669.

[20] Kanamori H, Mori J, Harkrider DG (1994) Excitation of atmospheric oscillations by volcanic eruptions. J Geophys Res 99:21947–21961

[21] Lin, J.-T., Rajesh, P. K., Lin, C. C. H., Chou, M.-Y., Liu, J.-Y., Yue, J., . . . Kung, M.-M. (2022). Rapid Conjugate Appearance of the Giant Ionospheric Lamb Wave in the Northern Hemisphere After Hunga-Tonga Volcano Eruptions. Earth and Space Science Open Archive, 18. Retrieved from https://doi.org/10.1002/essoar.10510440.2 doi: 10.1002/essoar.10510440.2

[22] Mikumo, T. and Bolt, B. A. (1985). Excitation mechanism of atmospheric pressure waves from the 1980 Mount St Helens eruption. Geophysical Journal International 81, 445–461

[23] Miller, S. D., Straka, W. C., Yue, J., Smith, S. M., Alexander, M. J., Hoffmann, L., et al. (2015). Upper atmospheric gravity wave details revealed in nightglow satellite imagery. Proceedings of the National Academy of Sciences of the United States of America, 112(49), E6728–E6735. https://doi.org/10.1073/pnas.1508084112

[24] Ogawa, T., Kumagai, H., & Sinno, K. (1982). Ionospheric disturbances over Japan due to the 18 May 1980 eruption of Mount St. Helens. Journal of Atmospheric and Terrestrial Physics, 44(10), 863-868.

[25] Otsuka, S. Visualizing Lamb waves from a volcanic eruption using meteorological satellite Himawari-8. Geophysical Research Letters, e2022GL098324.

[26] Picone, J. M., A. E. Hedin, D. P. Drob, and A. C. Aikin (2002), NRLMSISE-00 empirical model of the atmosphere: Statistical comparisons and scientific issues, J. Geophys. Res., 107(A12), 1468, doi:10.1029/2002JA009430.

[27] Saito, S. (2022). Ionospheric disturbances observed over Japan following the eruption of Hunga Tonga-Hunga Ha'apai on 15 January 2022. Earth, Planets and Space, 74(1), 1-9.

[28] Savitzky, A. and Golay, M. J. E. (1964). Smoothing and differentiation of data by simplified least squares procedures. Analytical Chemistry 36, 1627−1639

[29] Schmit, T. J., Griffith, P., Gunshor, M. M., Daniels, J. M., Goodman, S. J., & Lebair, W. J. (2017). A closer look at the ABI on the GOES-R series. Bulletin of the American Meteorological Society, 98(4), 681-698.

[30] Themens, D. R., Watson, C., Žagar, N., Vasylkevych, S., Elvidge, S., McCaffrey, A., ... & Jayachandran, P. T. (2022). Global propagation of ionospheric disturbances associated with the 2022 Tonga Volcanic Eruption. Geophysical Research Letters, e2022GL098158.

[31] Tsunoda, R. T. (2010). On seeding equatorial spread F: Circular gravity waves. Geophysical Research Letters, 37(10). https://doi.org/10.1029/2010GL043422

[32] Wright, C., Hindley, N., Alexander, M. J., Barlow, M., Hoffmann, L., Mitchell, C., et al. (2022). Surface-to-space atmospheric waves from Hunga Tonga-Hunga Ha'apai eruption. Earth and Space Science Open Archive. https://www.essoar.org/doi/10.1002/essoar.10510674.2

[33] Zhang S-R, Vierinen J, Aa E, Goncharenko LP, Erickson PJ, Rideout W, Coster AJ and Spicher A (2022) 2022 Tonga Volcanic Eruption Induced Global Propagation of Ionospheric Disturbances via Lamb Waves. Front. Astron. Space Sci. 9:871275. doi: 10.3389/fspas.2022.871275

[34] Zhang, S. R., Coster, A. J., Erickson, P. J., Goncharenko, L. P., Rideout, W., & Vierinen, J. (2019). Traveling ionospheric disturbances and ionospheric perturbations associated with solar flares in September 2017. Journal of Geophysical Research: Space Physics, 124(7), 5894-5917.

[35] Zhang, S. R., Erickson, P. J., Gasque, L. C., Aa, E., Rideout, W., Vierinen, J., ... & Coster, A. J. (2021). Electrified postsunrise ionospheric perturbations at Millstone Hill. Geophysical Research Letters, 48(18), e2021GL095151.

[36] Zhang, S. R., Erickson, P. J., Goncharenko, L. P., Coster, A. J., Rideout, W., & Vierinen, J. (2017). Ionospheric bow waves and perturbations induced by the 21 August 2017 solar eclipse. Geophysical Research Letters, 44(24), 12-067.

405
406

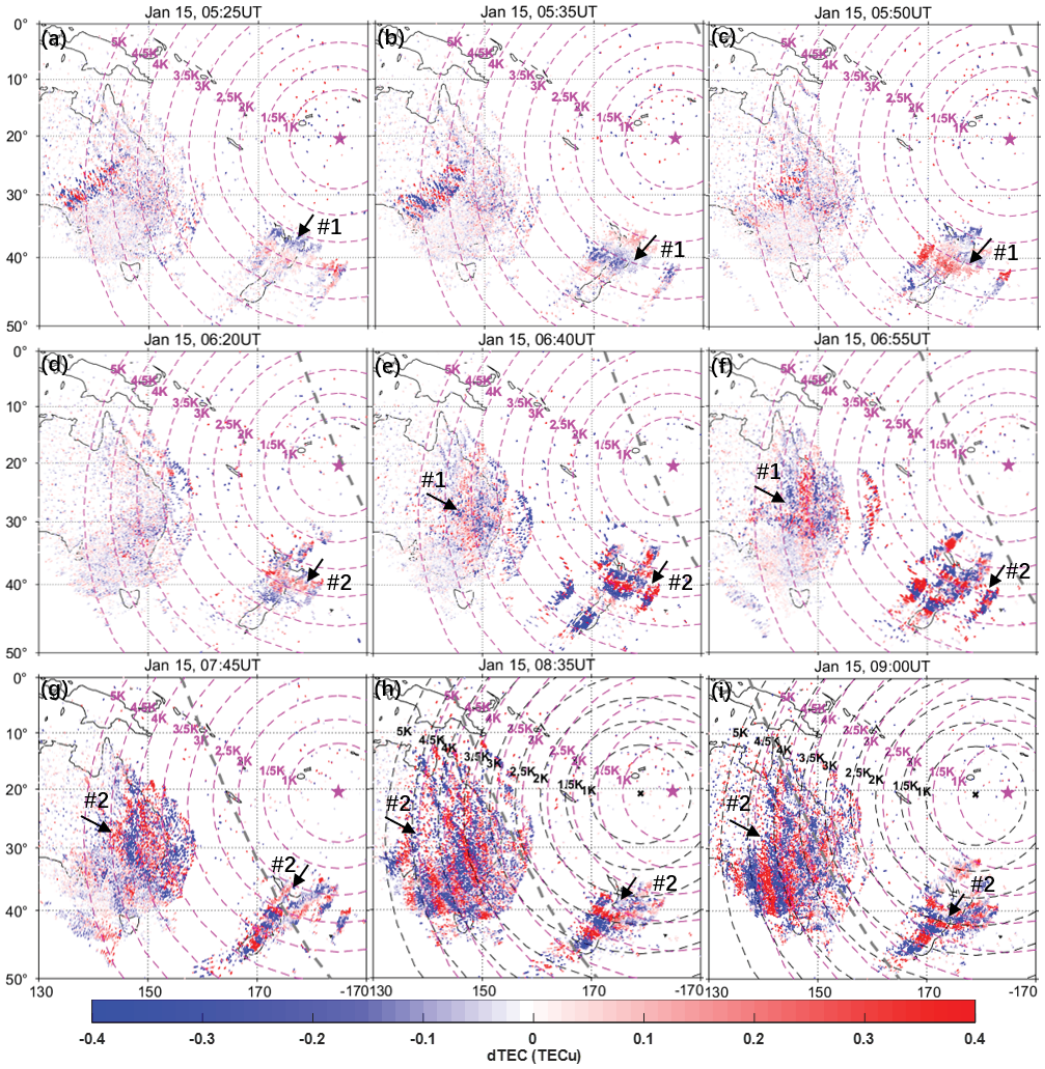

Figure 1. 2D maps of dTEC at nine selected time steps from 05:25 UT to 9:00 UT on January 15, 2022. The magenta star represents the Tonga volcanic eruption epicenter (20.5°S, 175.1°W). The black cross in panels (h) and (i) corresponds to the location of the "ionosphere disturbance center" (21.1°S, 178.6°E), which is fitted based on the wavefront of dTEC maps after 08:35 UT (see details in Figure S2 and Table S1 in the SI file). The iso-distance circles separated at 500 (0.5K) km intervals marked by dashed magenta and black lines are the great circles at an altitude of 300 km from the location of the volcanic eruption and ionospheric disturbance center, respectively. The gray dashed line indicates the location of the solar terminator. Full sets of 15-minute 2D dTEC maps on January 15 are available in Movie S1 of the SI file.

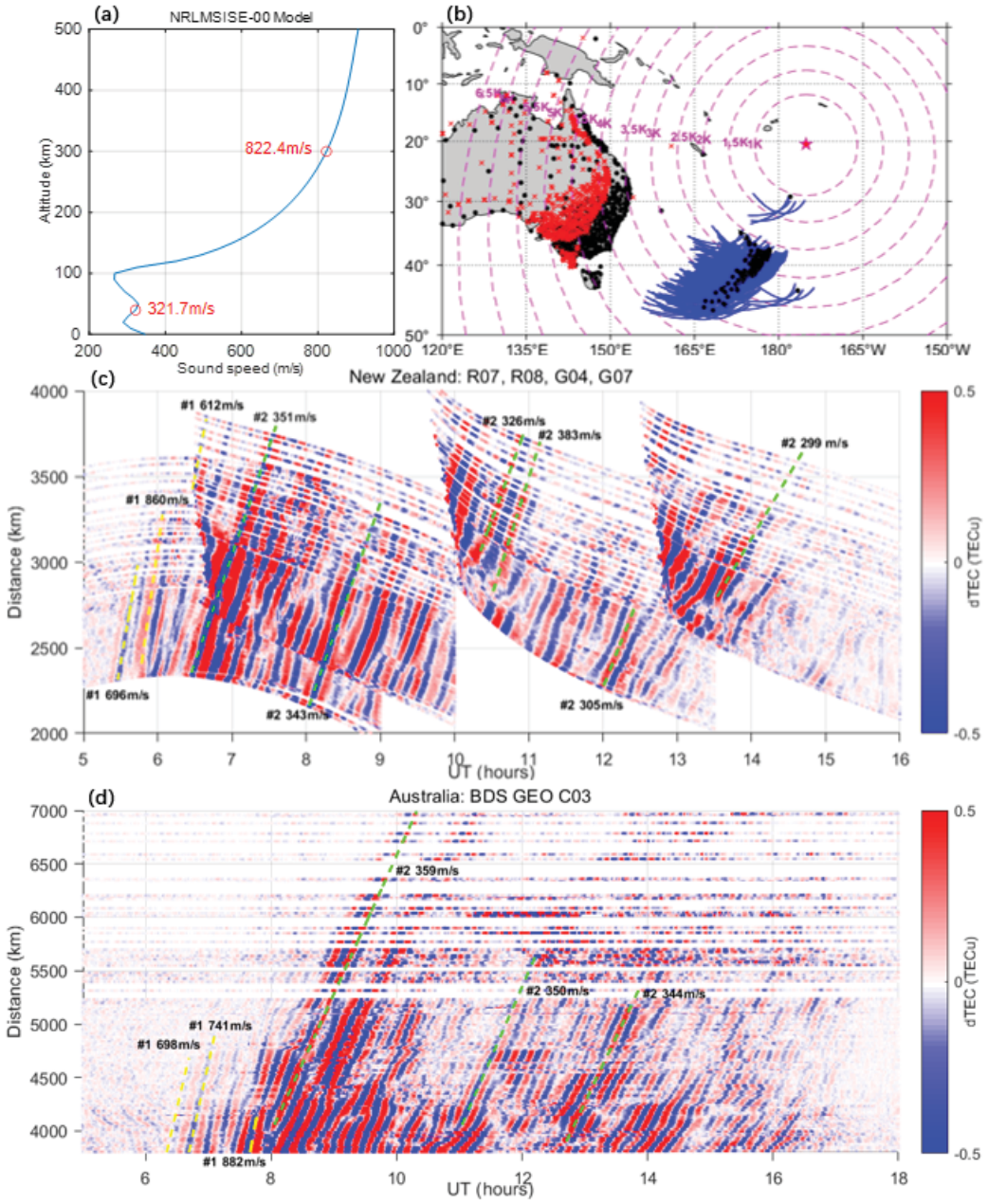

Figure 2. (a) The sound speed profile at various altitudes calculated from the NRLMSISE-00 model. The propagation speed at altitudes of 30 km and 300 km is marked by red circles. (b) IPP tracks over New Zealand and Australia. The blue curves and red crosses are the IPP locations derived from GNSS (GLONASS R07, R08, and GPS G04, G07) and BDS GEO (C03) satellites, respectively. The black dots are the locations of GNSS receivers. (c) The plot of the dTEC UT-distance from the volcanic eruption location for GLONASS (R07, R08) and GPS (G04, G07) satellites over New Zealand. (d) Similar to panel (c) but derived from BDS GEO C03 satellite over Australia. The CTID propagation velocity is marked by the oblique dashed black line in panels (c) and (d).

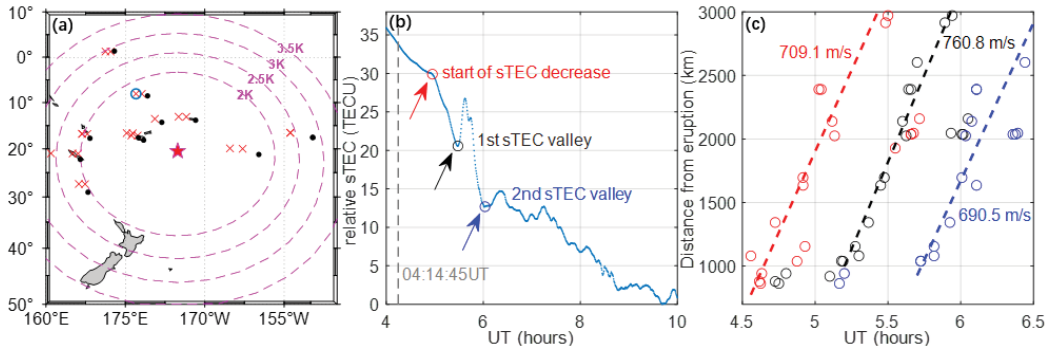

Figure 3. (a) BDS GEO satellite IPP distributions (red crosses) at the azimuth of -135° to 90° within 3000 km from the volcanic eruption location. These IPPs are calculated from BDS GEO satellites (C01 and C04) and available ground-based GNSS receivers in the area (shown as black dots). The cyan circle represents the IPP derived from the line of sight between GNSS receiver TUVA and BDS GEO C01. (b) An example of relative sTEC time series (cyan curves) between TUVA and C01. The time of sTEC starting to decrease, the first and second sTEC valleys are marked by red, black, and blue circles, respectively. The vertical dashed gray line represents the onset time of the Tonga volcanic eruption. (c) Arrival time of sTEC perturbations as a function of the distance from the volcanic eruption location. Red, black, and blue circles represent the arrival times of three types of ionosphere perturbations of the panel (b). Linear regression is performed to estimate the TID propagation speed, which is marked by oblique red/black/blue dashed lines.

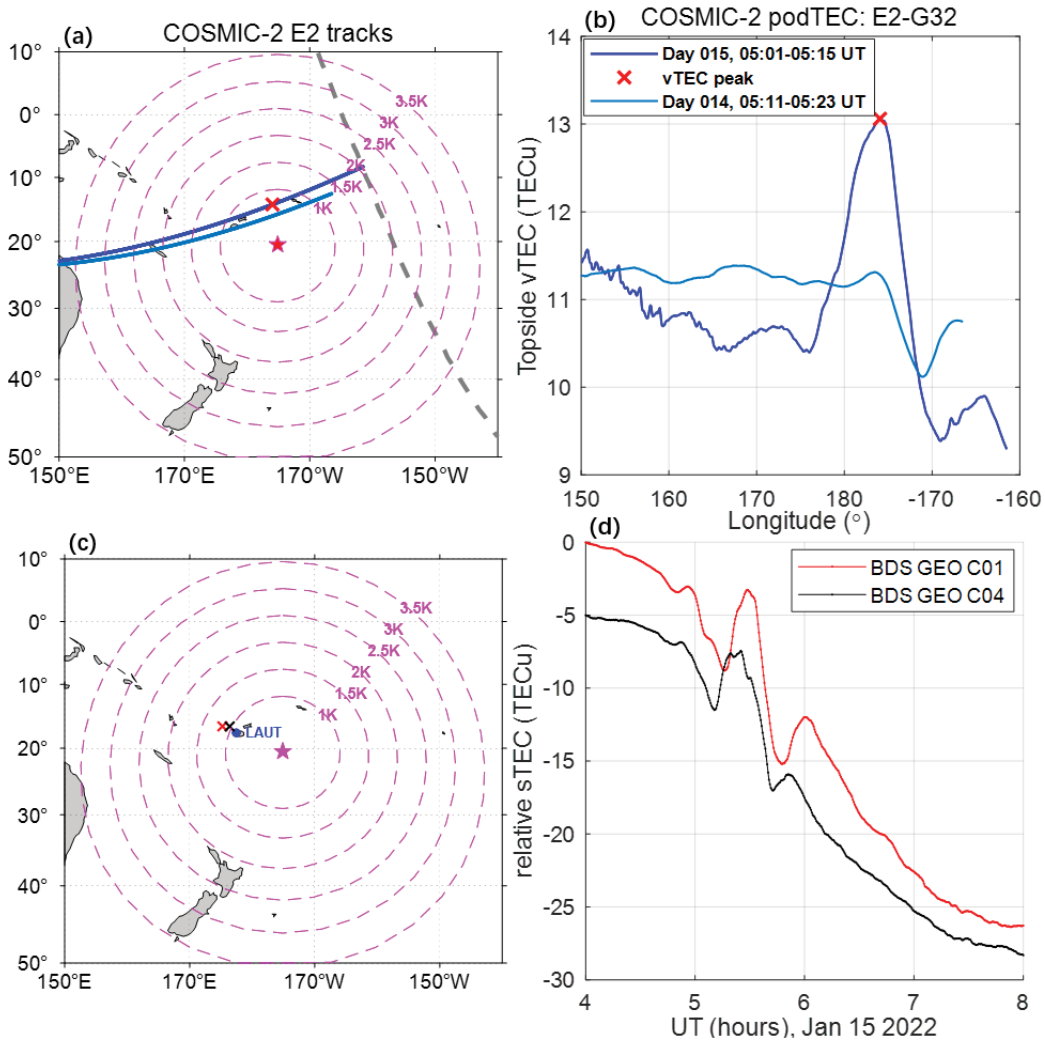

Figure 4. (a) COSMIC-2 E2 satellite tracks during 05:00-05:30 UT on January 15 (blue curves) and January 14 (cyan curves). The gray dashed line represents the solar terminator around 05:10 UT. (b) Topside podTEC variations during 05:00-05:30 UT for these two days. The TEC peak on January 15 is marked by the red cross in panels (a) and (b). (c) BDS GEO C01 (red cross) and C04 (black cross) IPP locations for LAUT station (blue dot). (d) Relative TEC temporal variations of BDS GEO C01 (red curve) and C04 (black curve) satellites during 04:00-08 UT on January 15, 2022.

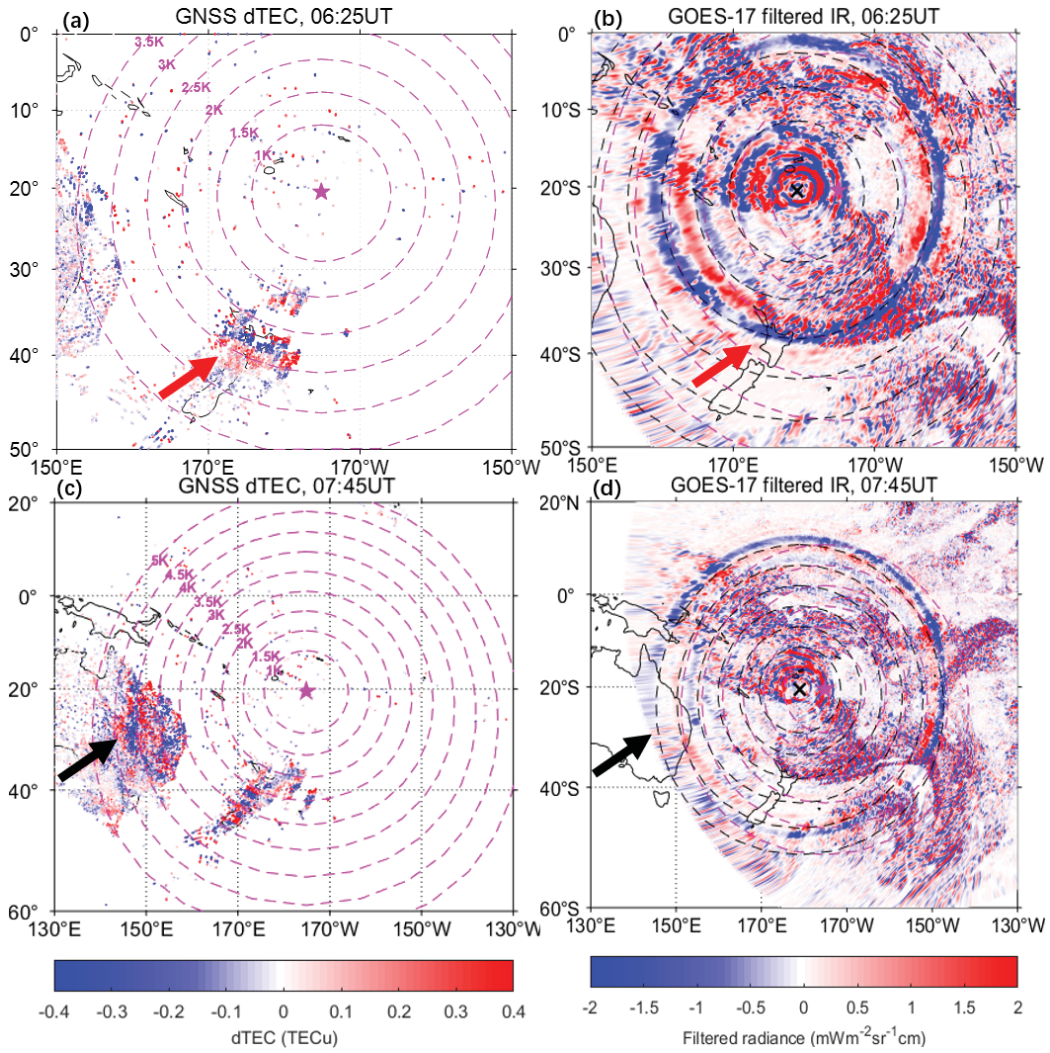

Figure 5. (a) CTID wavefronts at 300 km (ionospheric height) observed from GNSS dTEC maps at 06:25 UT on January 15, 2022. (b) Concentric Lamb waves at 30 km (stratospheric height) visualized by the GOES-17 filtered IR imagery at 06:25 UT on January 15, 2022. (c) and (d) Similar to (a) and (b), but at 7:45 UT. The dominant CTID and Lamb waves are marked by red arrows in (a) and (b) when arriving over New Zealand (06:25 UT), while they are marked by black arrows in (c) and (d) when arriving over Australia (7:45 UT). The volcanic eruption location and ionospheric disturbance center are marked by the magenta star and black crosses, respectively. Great circles altitude for GNSS dTEC (magenta dashed lines in panels (a) and (c)) and GOES-17 IR maps (magenta/black dash lines in panels (b) and (d)) are set to be 300 km and 30 km above the Earth, respectively.

Figure1.

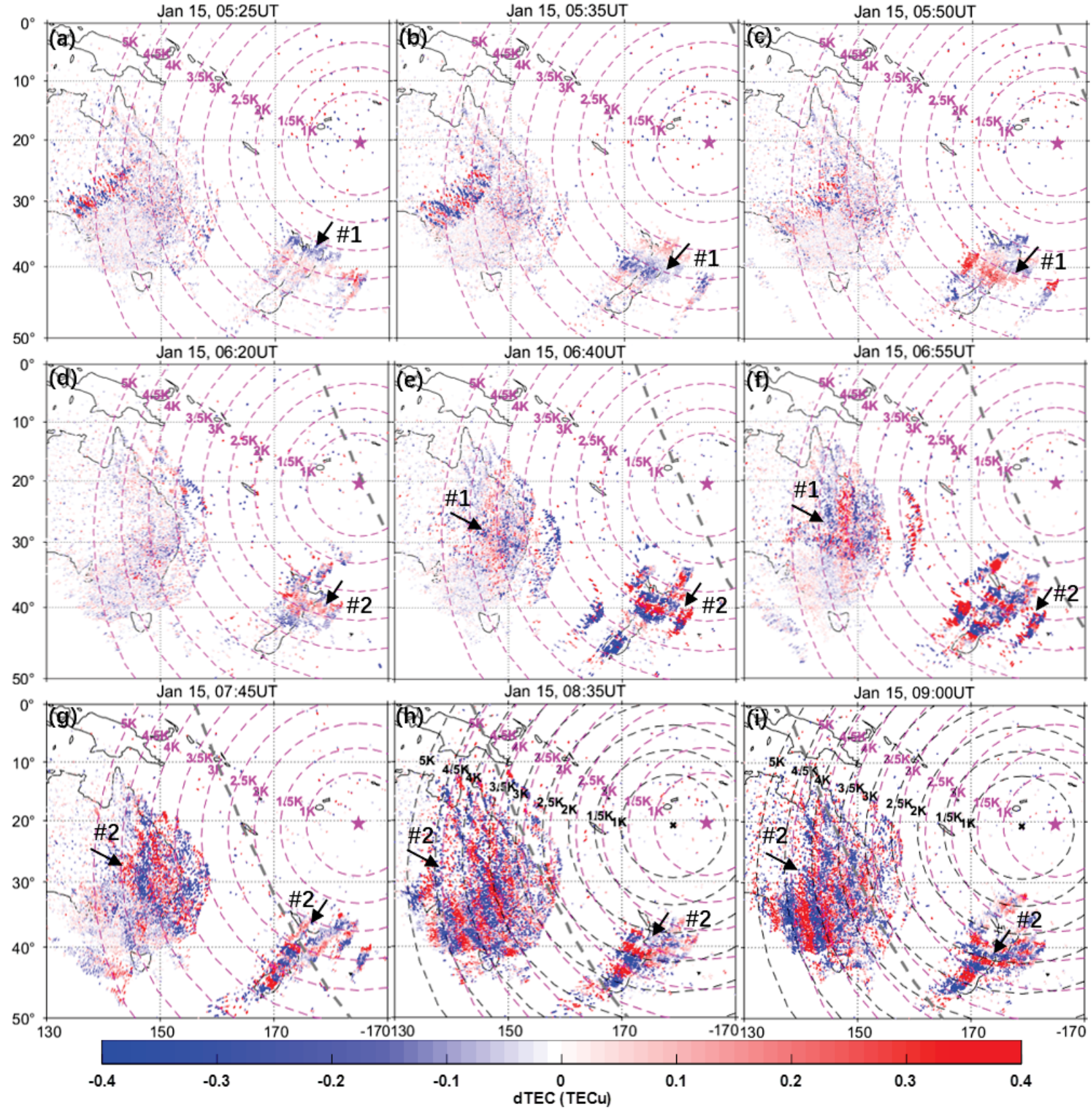
Jan 15, 05:25UT
Jan 15, 05:35UT
Jan 15, 05:50UT
Jan 15, 06:20UT
Jan 15, 06:40UT
Jan 15, 06:55UT
Jan 15, 07:45UT
Jan 15, 08:35UT
Jan 15, 09:00UT
(a)
(b)
(c)
(d)
(e)
(f)
(g)
(h)
(i)
#1
#2
0°
10°
20°
30°
40°
50°
130
150
170
-170
-0.4
-0.3
-0.2
-0.1
0
0.1
0.2
0.3
0.4
dTEC (TECu)

Figure2.

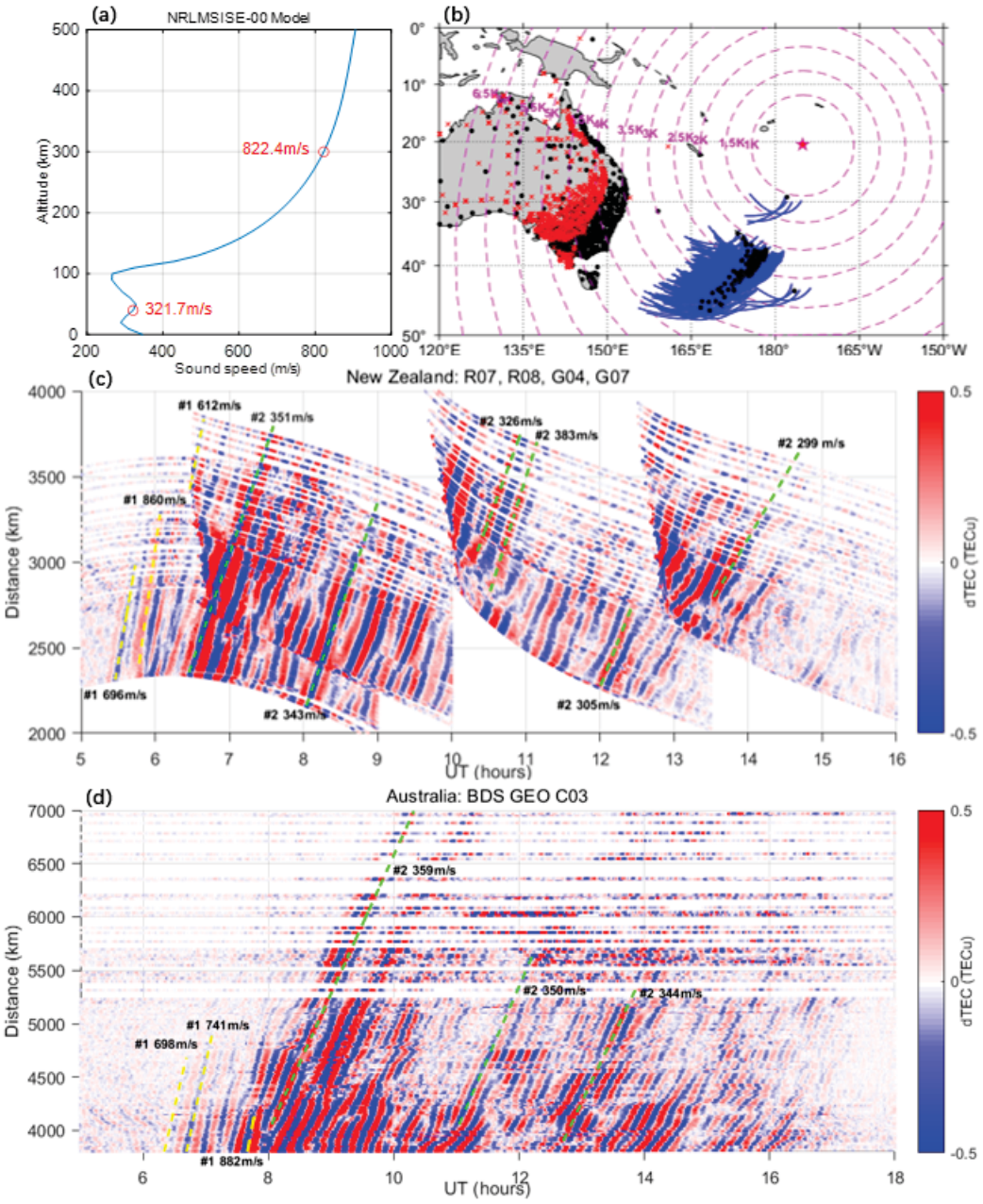
(a)
NRLMSISE-00 Model
822.4m/s
321.7m/s
Altitude (km)
Sound speed (m/s)
(b)
(c)
New Zealand: R07, R08, G04, G07
#1 612m/s
#2 351m/s
#2 326m/s
#2 383m/s
#2 299 m/s
#1 860m/s
#1 696m/s
#2 343m/s
#2 305m/s
Distance (km)
UT (hours)
dTEC (TECu)
(d)
Australia: BDS GEO C03
#2 359m/s
#2 350m/s
#2 344m/s
#1 741m/s
#1 698m/s
#1 882m/s
Distance (km)
UT (hours)
dTEC (TECu)

Figure3.

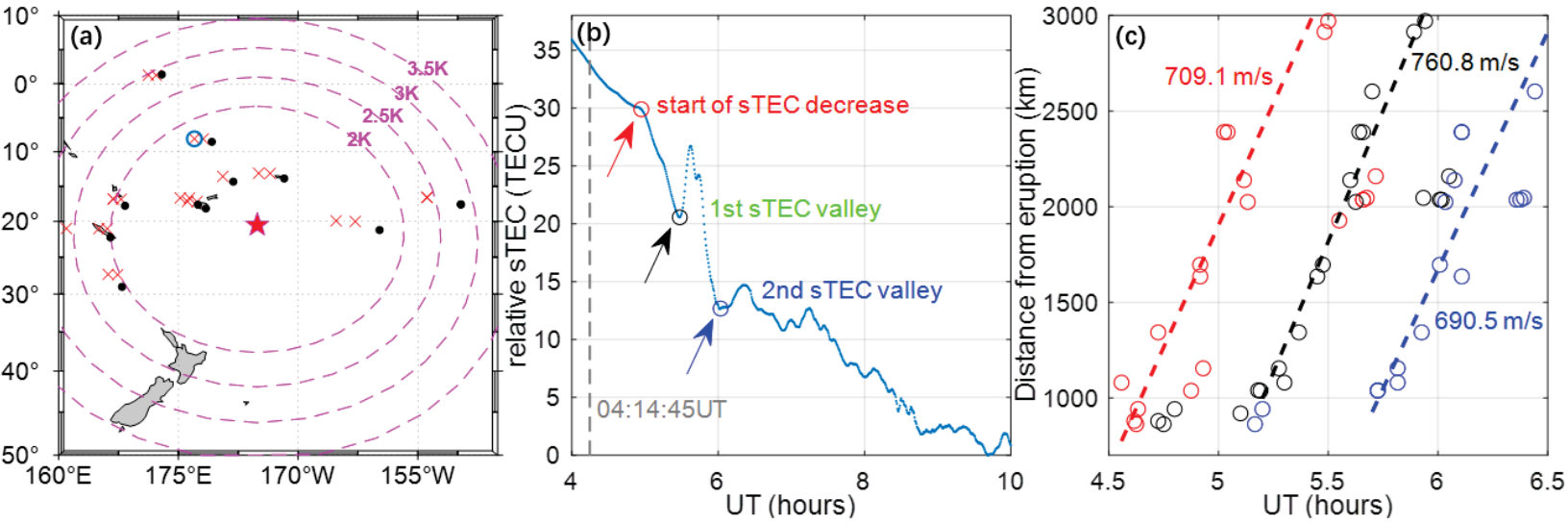
(a)
3.5K
3K
2.5K
2K
10°
0°
10°
20°
30°
40°
50°
160°E
175°E
170°W
155°W
(b)
relative sTEC (TECU)
start of sTEC decrease
1st sTEC valley
2nd sTEC valley
04:14:45UT
UT (hours)
(c)
Distance from eruption (km)
709.1 m/s
760.8 m/s
690.5 m/s
UT (hours)

Figure4.

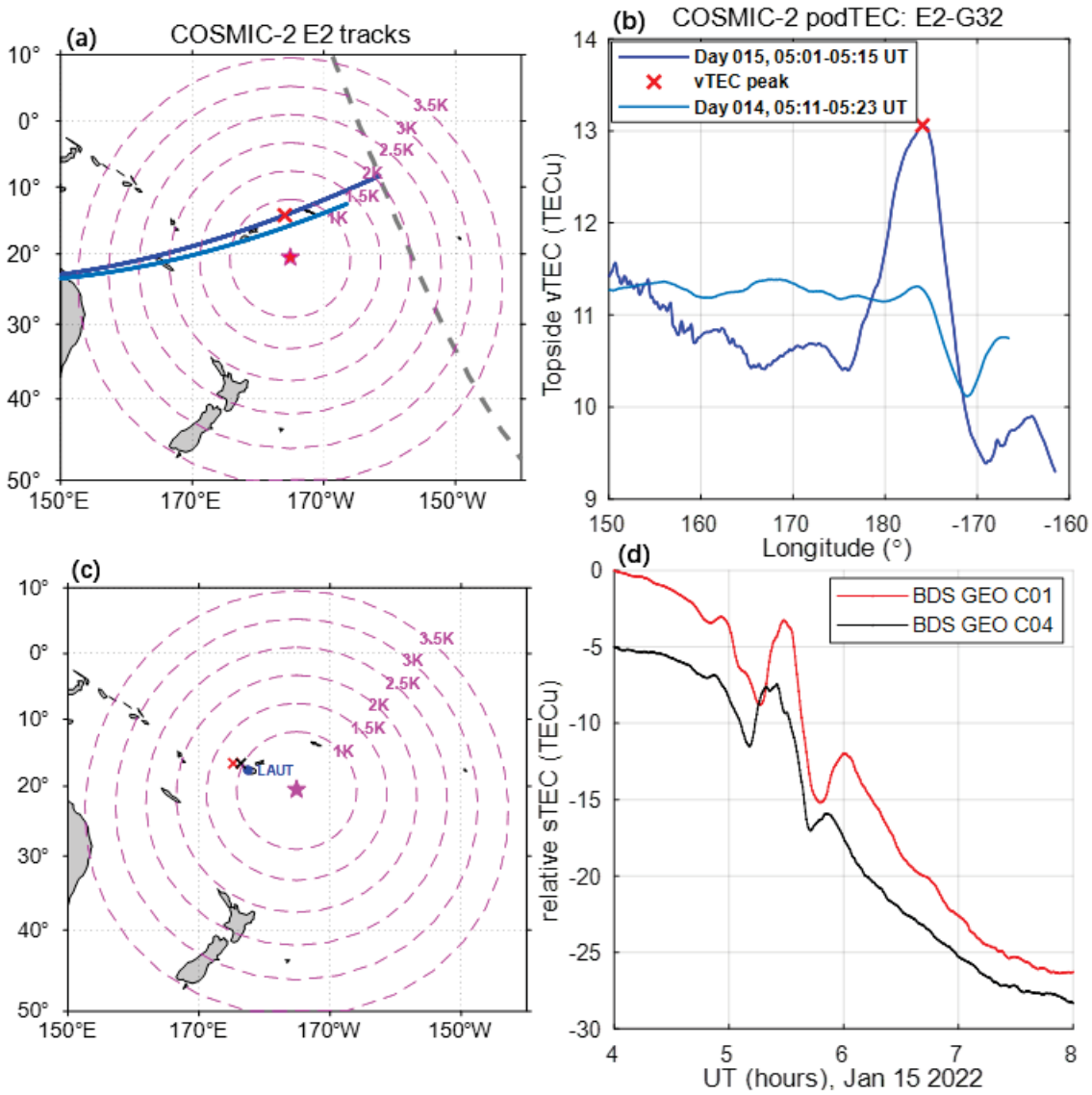
(a)
COSMIC-2 E2 tracks
10°
0°
10°
20°
30°
40°
50°
150°E
170°E
170°W
150°W
3.5K
3K
2.5K
2K
1.5K
1K
(b)
COSMIC-2 podTEC: E2-G32
Day 015, 05:01-05:15 UT
vTEC peak
Day 014, 05:11-05:23 UT
Topside vTEC (TECu)
14
13
12
11
10
9
150
160
170
180
-170
-160
Longitude (°)
(c)
LAUT
(d)
BDS GEO C01
BDS GEO C04
relative sTEC (TECu)
0
-5
-10
-15
-20
-25
-30
4
5
6
7
8
UT (hours), Jan 15 2022

Figure5.

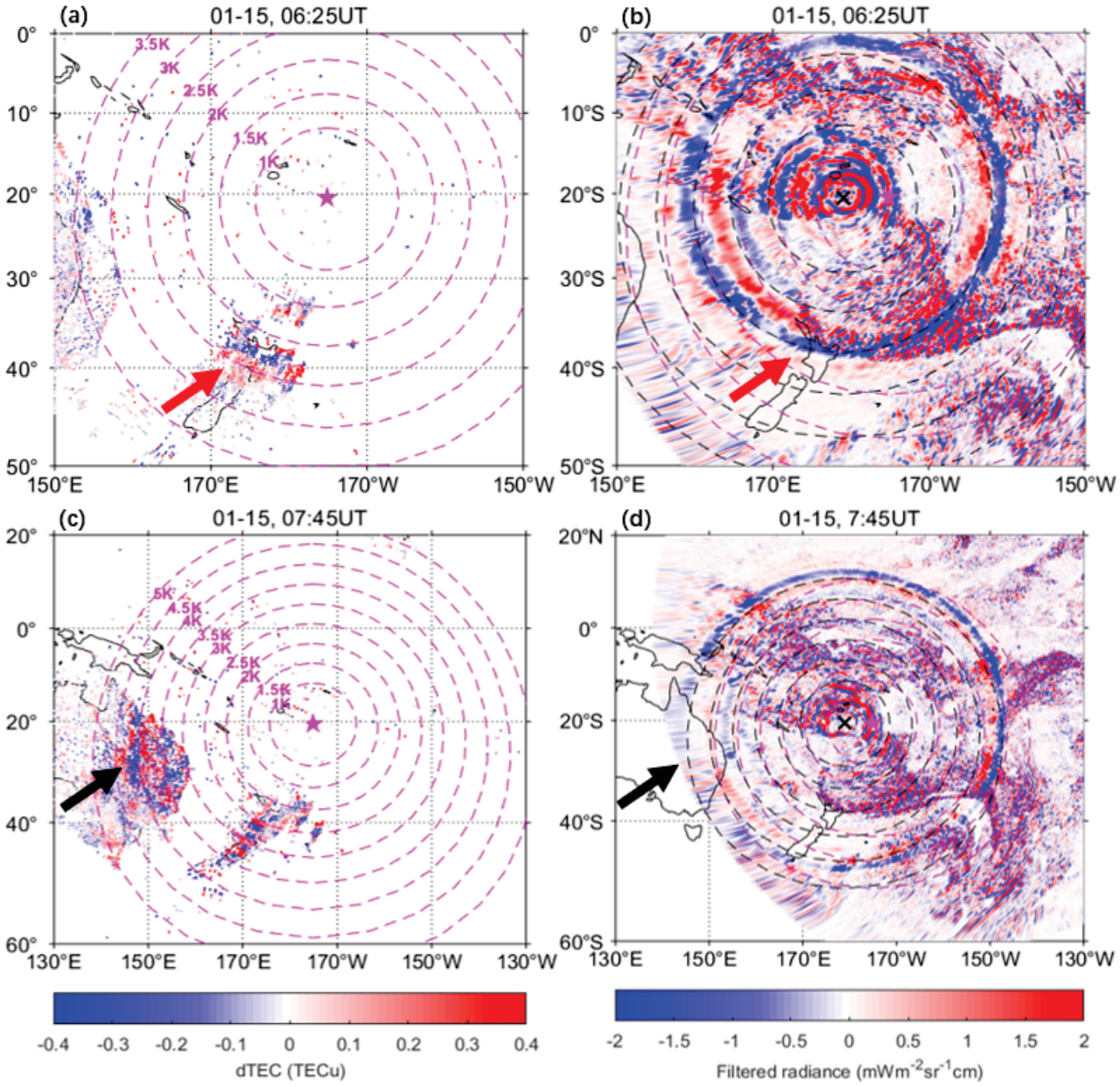
(a)
01-15, 06:25UT
3.5K
3K
2.5K
2K
1.5K
1K
0°
10°
20°
30°
40°
50°
150°E
170°E
170°W
150°W
(b)
01-15, 06:25UT
0°
10°S
20°S
30°S
40°S
50°S
150°E
170°E
170°W
150°W
(c)
01-15, 07:45UT
5K
4.5K
4K
3.5K
3K
2.5K
2K
1.5K
1K
20°
0°
20°
40°
60°
130°E
150°E
170°E
170°W
150°W
130°W
(d)
01-15, 7:45UT
20°N
0°
20°S
40°S
60°S
130°E
150°E
170°E
170°W
150°W
130°W
-0.4
-0.3
-0.2
-0.1
0
0.1
0.2
0.3
0.4
dTEC (TECu)
-2
-1.5
-1
-0.5
0
0.5
1
1.5
2
Filtered radiance (mWm-2sr-1cm)